TÜBİTAK

Turkish Journal of Chemistry

http://journals.tubitak.gov.tr/chem/

Research Article

Turk J Chem
(2021) 45: 295-306
© TÜBİTAK
doi:10.3906/kim-2008-46

Enhanced ethanol sensing properties of WO_3 modified TiO_2 nanorods

Bekzat ABDIKADYR, Alp KILIÇ, Onur ALEV, Serkan BÜYÜKKÖSE, Zafer Ziya ÖZTÜRK*
Department of Physics, Faculty of Science, Gebze Technical University, Kocaeli, Turkey

Received: 27.08.2020 • **Accepted/Published Online:** 08.12.2021 • **Final Version:** 27.04.2021

Abstract: Pristine and WO_3 decorated TiO_2 nanorods (NRs) were synthesised to investigate n-n-type heterojunction gas sensing properties. TiO_2 NRs were fabricated via hydrothermal method on fluorine-doped tin oxide coated glass (FTO) substrates. Then, tungsten was sputtered on the TiO_2 NRs and thermally oxidised to obtain WO_3 nanoparticles. The heterostructure was characterised by X-ray diffraction (XRD), scanning electron microscopy (SEM), and energy-dispersive X-ray (EDX) spectroscopy. Fabricated sensor devices were exposed to VOCs such as toluene, xylene, acetone and ethanol, and humidity at different operation temperatures. Experimental results demonstrated that the heterostructure has better sensor response toward ethanol at 200 °C. Enhanced sensing properties are attributed to the heterojunction formation by decorating TiO_2 NRs with WO_3.

Key words: WO_3/TiO_2, gas sensor, heterostructure, nanorods, ethanol

1. Introduction

Volatile organic compounds (VOCs) such as ethanol, acetone, toluene, xylene have been widely used in daily life, especially in industrial applications. However, VOCs induce some harmful effects for human health and environment [1-6]. In addition, some VOCs have been referred as tracer compounds in the human exhaled breath for various diseases [7-9]. Moreover, ethanol is the strongest indicator for detection of alcohol level in human breath [10]. Therefore, proper and fast detection of various VOCs is very important for different applications such as, traffic security, environmental monitoring, in-door air quality and breath analysis.

There are many detection techniques for VOCs such as optical, spectroscopic, chromatographic, electrochemical [11-13]. Among all these techniques, semiconductor metal oxide (SMO) based chemi-resistive gas sensors are one of the best candidates due to their high sensitivity and easy production processes [14-16]. Moreover, different techniques such as loading with a catalyst, doping a host element, or heterostructural fabrication of SMO materials may improve their gas sensing properties against various gas species [17-22]. Therefore, SMOs are superior sensing materials for VOCs detection.

As an n-type semiconductor, TiO_2 is one of the most used material for VOCs detection for many years. TiO_2 has some distinctive features such as its nontoxic nature, easy nanostructural fabrication, and superior reaction ability to a wide range of VOCs. Especially, one dimensional (1D) TiO_2 nanomaterials such as nanorods and nanotubes have been widely used due to their higher surface-to-volume ratio [23-27]. However, some sensor properties such as selectivity and operation temperature must be still improved for specific applications. Therefore, scientists are interested in hetero-structured metal oxides such as TiO_2, to increase their sensing performances. The sensing performances of heterojunction enhance in virtue of band alteration at the interface between different materials. This provides charge transfer through the interface from one material to another by creating charge-space region and adsorption sites [17, 28-32]. WO_3 is one of the best candidates for heterostructure due to its highly reactive nature against various VOCs [33,34]. WO_3/TiO_2 heterostructures have been widely investigated for photocatalytic, thermochromic and supercapacitor applications [35-37]. However, investigation of gas sensing properties of WO_3/TiO_2 heterostructures is still limited. L.E. Depero et al. [38] and D-S. Lee et al. [39] fabricated TiO_2-WO_3 sensors with sputtering and coprecipitation methods, respectively, and explored their NO_3 sensing performances. Y. Yao et al. [40] fabricated TiO_2-WO_3 composite coatings and explained the enhanced methane sensing properties by creation of heterojunctions between the TiO_2 and WO_3 interface. S.M. Zanetti et al. investigated the WO_3 doping effect on TiO_2 nanocrystalline powders and estimated their excellent humidity sensing properties [41]. W. Meng et al. synthesised TiO_2 powder-core WO_3 shell composite sensing electrode and demonstrated

* Correspondence: zozturk@gtu.edu.tr

a better NH_3 sensing performance [42]. Even though, MOX heterostructures have potential applications in chemical gas sensors [43-45], there are limited study on the sensing properties of WO_3/TiO_2 NRs heterostructures. Especially, studies with various WO_3 loading are considerably poor.

In this study, WO_3/TiO_2 NRs with various WO_3 loading were obtained for chemical gas sensors. The enhancing sensor performance of SMO gas sensors with decorating of highly ordered 1D n-type TiO_2 NRs by n-type WO_3 is the motivation of this study. Highly ordered TiO_2 NRs were synthesised by hydrothermal method on TiO_2 seed-layer coated FTO substrates. Then, WO_3 layers were coated on TiO_2 NRs by magnetron sputtering technique with different thicknesses. Structural and morphological characterisation of WO_3/TiO_2 heterostructures were investigated. Gas sensor performances of heterostructures were studied against ethanol, toluene, xylene, acetone and humidity at various temperatures.

2. Materials and methods

FTO substrates (8 Ω/sq) was obtained from Sigma-Aldrich (ChemieGmbH, Hamburg, Germany). Hydrochloric acid (HCl, 37%) was acquired from Sigma-Aldrich. Titanium (IV) isopropoxide (TTIP, 97 +%) and sodium tungsten oxide dihydrate ($Na_2WO_3 \cdot 2H_2O$, 95%, crystalline) were provided from Alfa Aesar (city, country?). Titanium target (Ti, 99.995% purity and 2.00" diameter × 1.25" thick) and tungsten target (W, 99.95% purity and 2.00" diameter × 1.25" thick) were purchased from Kurt J. Lesker Company (city, country?). Distilled (DI) water (18 MΩ) was utilised through the all experiments.

2.1. Fabrication of WO_3 modified TiO_2 NRs heterostructures

The WO_3/TiO_2 heterostructures were obtained on the basis of different studies in the literature. A compact TiO_2 seed-layer with a thickness of approximately 50 nm was deposited on the FTO substrate to prevent shorting before the growth of TiO_2 NRs as reported previously in literature [46]. First, FTO substrates were purified by acetone, isopropanol and DI water in ultrasonic bath for 10 min, respectively. Then, Ti seed-layer was deposited by RF magnetron sputtering on the FTO substrates. Sputtering of Ti thin film (TF) process was performed in 5m Torr Ar atmosphere, with applied power of 100 W for 25 min. Finally, samples were annealed in the air atmosphere at 500 ˚C for 3 h. During the thermal oxidation process, Ti layer reacts with oxygen molecules in the air and transforms to TiO_2 layer [47].

TiO_2 NRs were synthesised by hydrothermal method on TiO_2 seed-layer coated FTO substrates. Firstly, 40 mL DI water and 40 ml HCl was mixed. Then, 0.9 ml TTIP was added drop by drop on previously mixed solution. Finally, the resulting mixture was stirred for 1 h at room temperature to obtain a homogeneous solution. This precursor solution was poured into a 250 mL autoclave, and TiO_2 seed-layer coated FTO substrates were placed vertically into the autoclave. Then the autoclave was sealed, placed into the temperature-controlled oven and thermally treated at 170 °C for 15 h [22, 48]. After thermal treatment, the samples were removed from autoclave, rinsed in DI water and dried under dry air flow.

WO_3 layer was deposited on TiO_2 NRs by the thermal oxidation method. Firstly, W layer was deposited by RF magnetron sputtering. Deposition of W layer was performed at 5 m Torr with RF power of 120 W for 1, 2, and 3 min under Ar atmosphere. Then, deposited W layer was thermally oxidised at 450 °C for 1 h to obtain the WO_3 layer [49]. Sensor fabrication process was illustrated in Figure 1. Pristine TiO_2 NRs sample was named as TiO_2, and WO_3-modified TiO_2 NRs samples were named as WT-1, WT-2 and WT-3 in accordance with W deposition time of 1, 2, and 3 min, respectively.

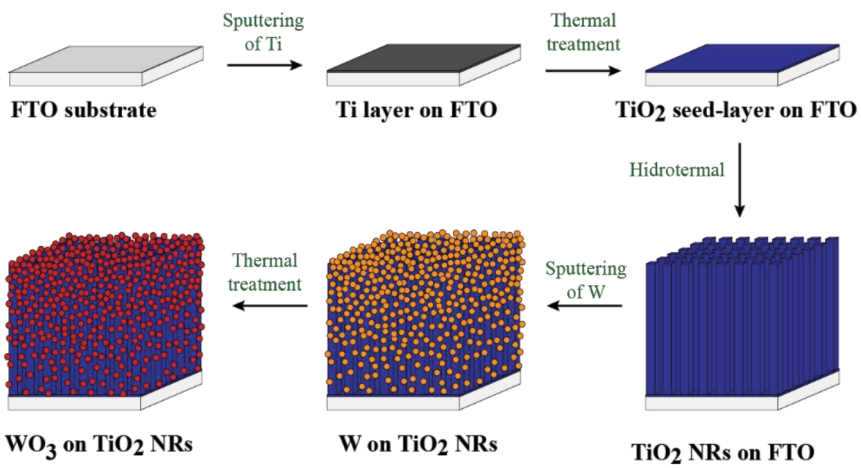

Figure 1. Schematic illustration of WO_3/TiO_2 NRs fabrication process.

The morphological and structural characterisations of fabricated samples were performed by scanning electron microscopy (SEM) equipped with energy dispersive X-ray spectroscopy (EDX) (Philips XL 30S) and X-ray diffraction (XRD) (Rigaku D-max, RINT-2200 series, X-ray diffractometer with Cu-Kα radiation, λ = 0.15418 nm), respectively.

2.2. Gas sensing measurements

WO_3-decorated TiO_2 NRs were examined for VOCs and humidity sensing performance. To perform electrical measurements, aluminium contact electrodes (thickness 200 nm) were evaporated on the samples with Leybold Univex 450 (city, country?) thermal evaporation system. Schematic illustration of sensor fabrication was given in Figures 2a and 2b. The sensors were placed into a test chamber with 1 L in volume. A high purity dry airline was connected to the test chamber. The dry air flow and the concentration of gases were controlled by flow meters and a multi gas controller – MKS 647C. Working temperature of devices was controlled by a Lakeshore 340 (city, country?). Keithley 6517A electrometer (city, country?) was used for current vs. time characteristics during gas sensing measurements. The atmosphere in the test chamber was cleaned by dry air flow. When the electric current reached a steady value, VOCs was sent to the test chamber. Humidity sensing performances of the sensors were also characterised. VOCs were generated by bubbling method [25]. Antoine's equation was used to calculate VOCs' concentration. All data were reported as a sensor response defined as follows [50];

$S_R = \Delta I / I_0$,

where ΔI is the change in the current value when sensors were exposed to target gas molecules, I_0 is the baseline current value measured under dry air flow condition. Response ($t90_{res}$) and recovery ($t90_{rec}$) times are defined as the time required the sensor to achieve 90% ΔI of its current form [51,52].

3. Results and discussion

3.1. Material characterisation

The surface morphology and elemental analysis were performed by SEM and EDX, respectively. The SEM images indicate that TiO_2 NRs are vertically aligned and homogenously covered on the substrate surface as seen in Figure 3a. The NRs were approximately 100 nm in diameter and 4.18 μm in length (Figure 3a inset). Figures 3b-3d show increasing amount of WO_3 layer on the TiO_2 NRs. The amount of WO_3 depends on W sputtering time.

Figure 4 shows the presence of the titanium, tungsten and oxygen in the rods. EDX spectrum of the samples in Figure 4a shows that tungsten is not present in TiO_2 sample and atomic distribution of W are 0.5%, 0.94% and 1.11% in WT-1, WT-2 and WT-3 samples, respectively. The amount of W particles is correlated with sputtering time of W. The EDX mapping of WT-3 is given in Figure 4b. W particles homogeneously covered the surface of TiO_2 NRs as seen in Figure 4b.

XRD patterns of the samples are given in Figure 5. According to the XRD patterns, the diffraction peaks 36.1° and 62.8° were attributed to (101) and (002) crystal planes of rutile TiO_2, respectively (PDF card number 00-021-1276). The intensity of the diffraction peaks 36.1° and 62.8°, which refer to rutile TiO_2, decrease in samples WT-1, WT-2 and WT-3. This can be explained by decorating of TiO_2 NRs with WO_3 [53]. In addition, there are no observed diffraction peaks related with WO_3 in the XRD pattern, which might be due to poor signal formation from small amount of material loading. In order to identify the WO_3 XRD pattern, WO_3 TF with a thickness of 50 nm (WO_3-50) was deposited by RF magnetron sputter system, and subsequently thermal oxidised on FTO substrate. In Figure 6 comparative XRD results are shown for WO_3-50, WT-3 and pristine FTO substrate. Diffraction peaks at $2\theta = 23.2^0$, 24.54^0, 33.1^0 and 34^0 can be assigned to monoclinic WO_3 (002), (200), (022) and (220) reflections, respectively (PDF card number 00-043-1035). The peaks which marked as "S" belong to FTO substrate (PDF card number 00-046-1088).

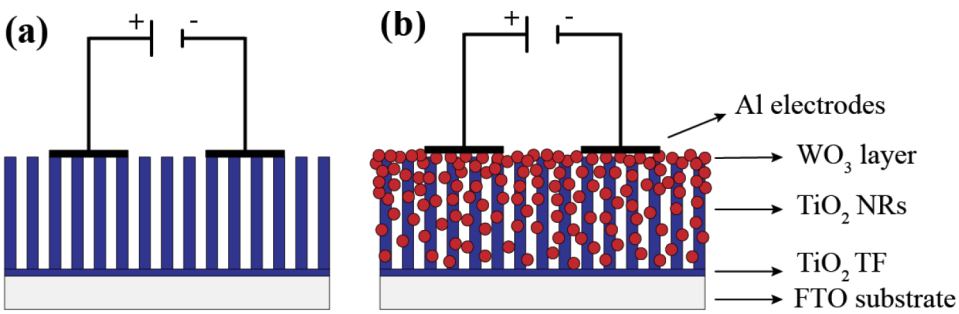

Figure 2. Schematic illustration of a) pristine TiO_2 NRs and b) WO_3 decorated TiO_2 heterostructure sensor devices.

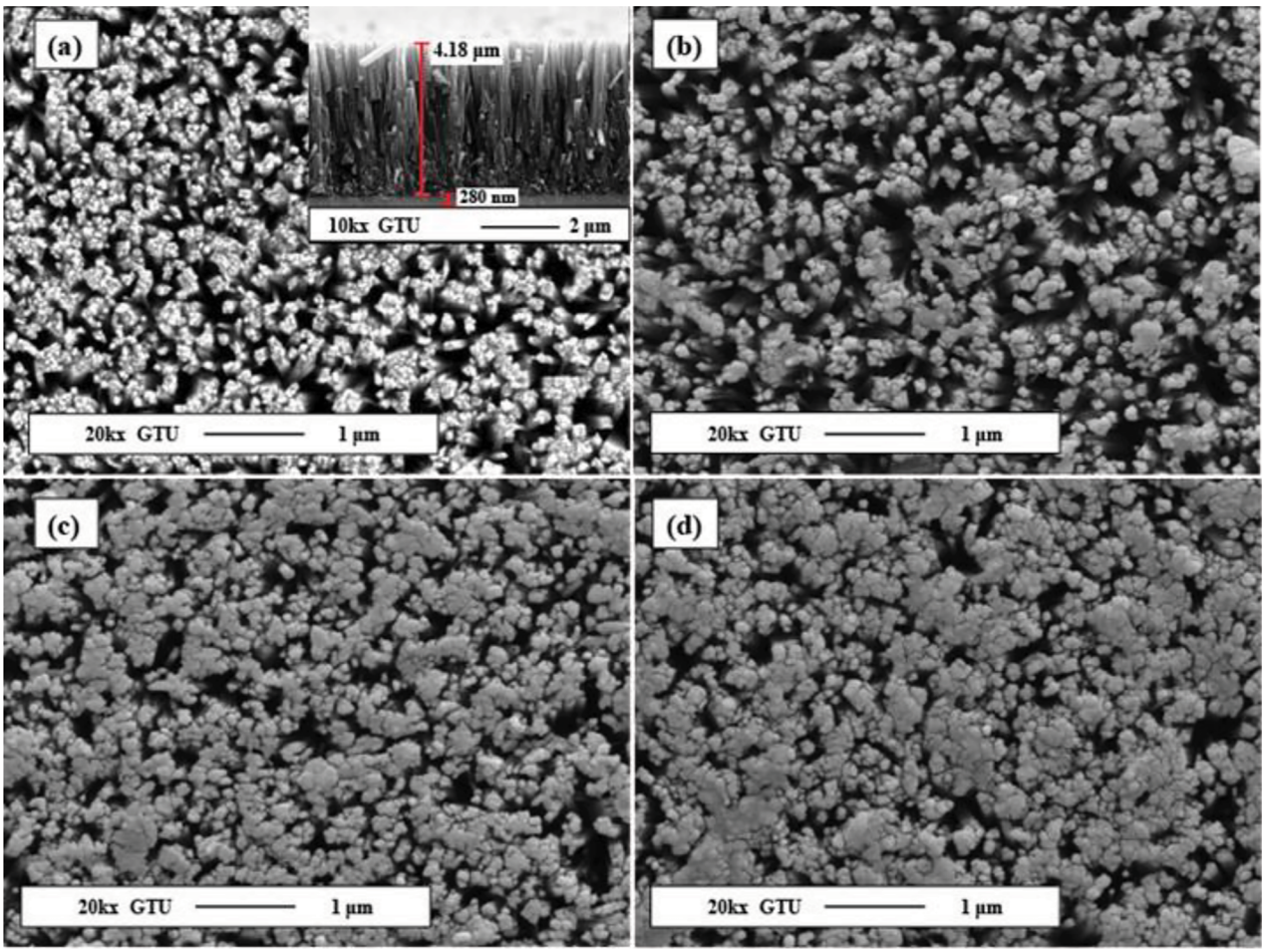

Figure 3. SEM images of a) TiO_2 NRs, b) WT-1, c) WT-2, and d) WT-3.

Growth of TiO_2 NRs can be explained with two continuous reactions;

$$Ti(OR)_4 + 4H_2O \rightarrow Ti(OH)_4 + 4ROH \qquad (hydrolysis)$$

$$Ti(OH)_4 \rightarrow TiO_2, xH_2O + (2-x)H_2O \qquad (condensation)$$

where R is ethyl, i-propyl, n-butyl, etc. [54].

Firstly, hydrolysis occurs by reaction of TiO_2 precursor (TTIP) with water and TTIP transforms to titanium alkoxide. Then, titanium alkoxide forms a complex with water. The acidic platform controls the rate of complex formation. Finally, the high temperature and pressure condition accelerates hydrolysis process and appeared complex starts to deposit onto the substrate as TiO_2 NRs in rutile phase [55]. The fundamental reason of growing highly ordered NRs in the deposition process of titanium complexes onto the substrate is surface energy. In the TiO_2 phase, the lowest surface energy has (110) face. It means that [001] direction, parallel to (110) plane, is the theoretically preferable growth direction. The powerful (002) pick in XRD pattern is the proof of the growth of the highly aligned TiO_2 NRs along [001] direction [56].

3.2. Gas sensing properties

Gas sensor measurements of fabricated sensors were performed under toluene, xylene, acetone, ethanol, and relative humidity ambient in an operation temperature range between 100 °C and 250 °C. There was no observed sensor response signal from all the samples against any gases at 100 °C. Also, pristine TiO_2 and WO_3/TiO_2 heterostructures could not sense acetone molecules for all operation temperatures. Operation temperature dependent sensor response results of all sensors are given in Figure 7 with bar diagrams.

After all sensor measurements at different operation temperatures, 200 °C is identified as the optimal operation temperature for all sensors due to the highest sensor response values against each gas. At the optimal operation temperature,

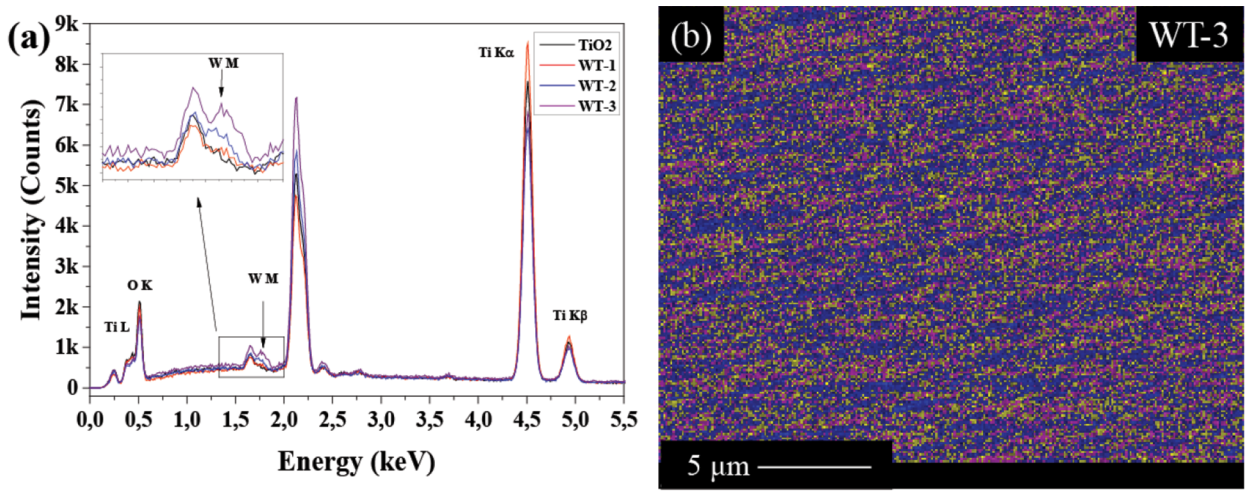

Figure 4. a) EDX spectrum of TiO_2, WT-1, WT-2, and WT-3 samples and b) EDX mapping of WT-3 sample. In the mapping image, O, Ti, and W were representing yellow, blue, and purple, respectively.

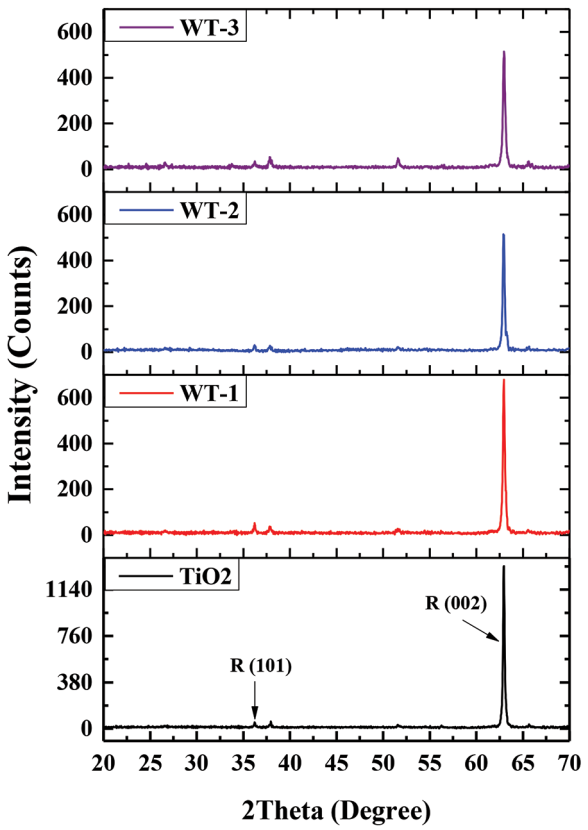

Figure 5. XRD patterns of the samples.

WT-1 sensor showed an excellent sensing performance against 1850 ppm ethanol as seen in Figure 7b. Sensor performance toward ethanol is drastically increased with the effect of WO_3 on the surface. Sensor response of WT-1 is 18-fold higher compared to pristine TiO_2 NRs at 200 °C. WO_3 plays a key role on the surface as catalyst and increases the sensor response. Also, sensor response values of WT-1 are highest against all tested gases due to catalytic effect of WO_3. After the identifying optimal operation temperature, concentration dependence of sensor response was investigated at 200 °C. Concentration dependence of sensor response is given in Figure 8.

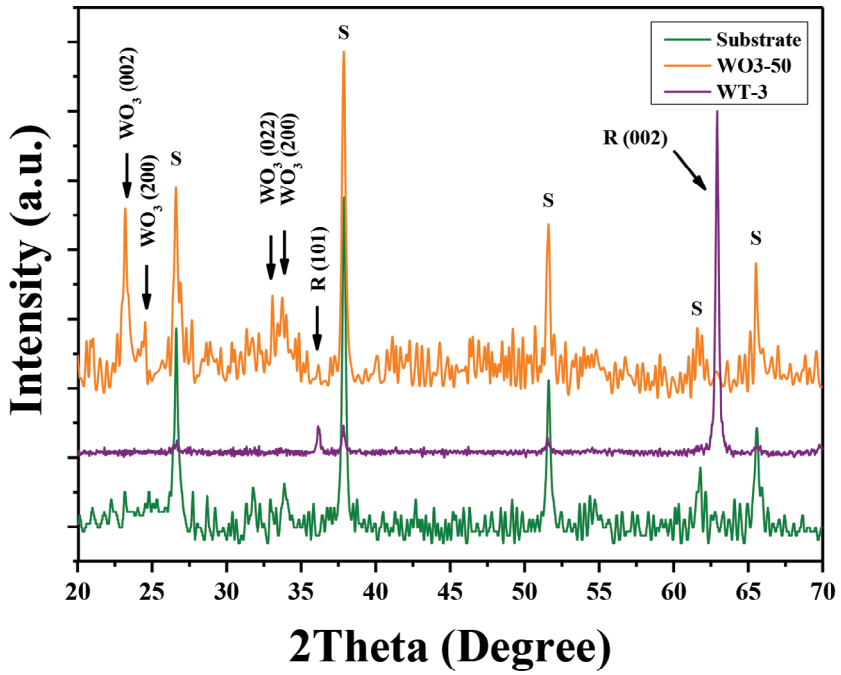

Figure 6. Comparison of XRD patterns of FTO substrate, 50 nm thick WO_3 thin film, and WT-3 sample.

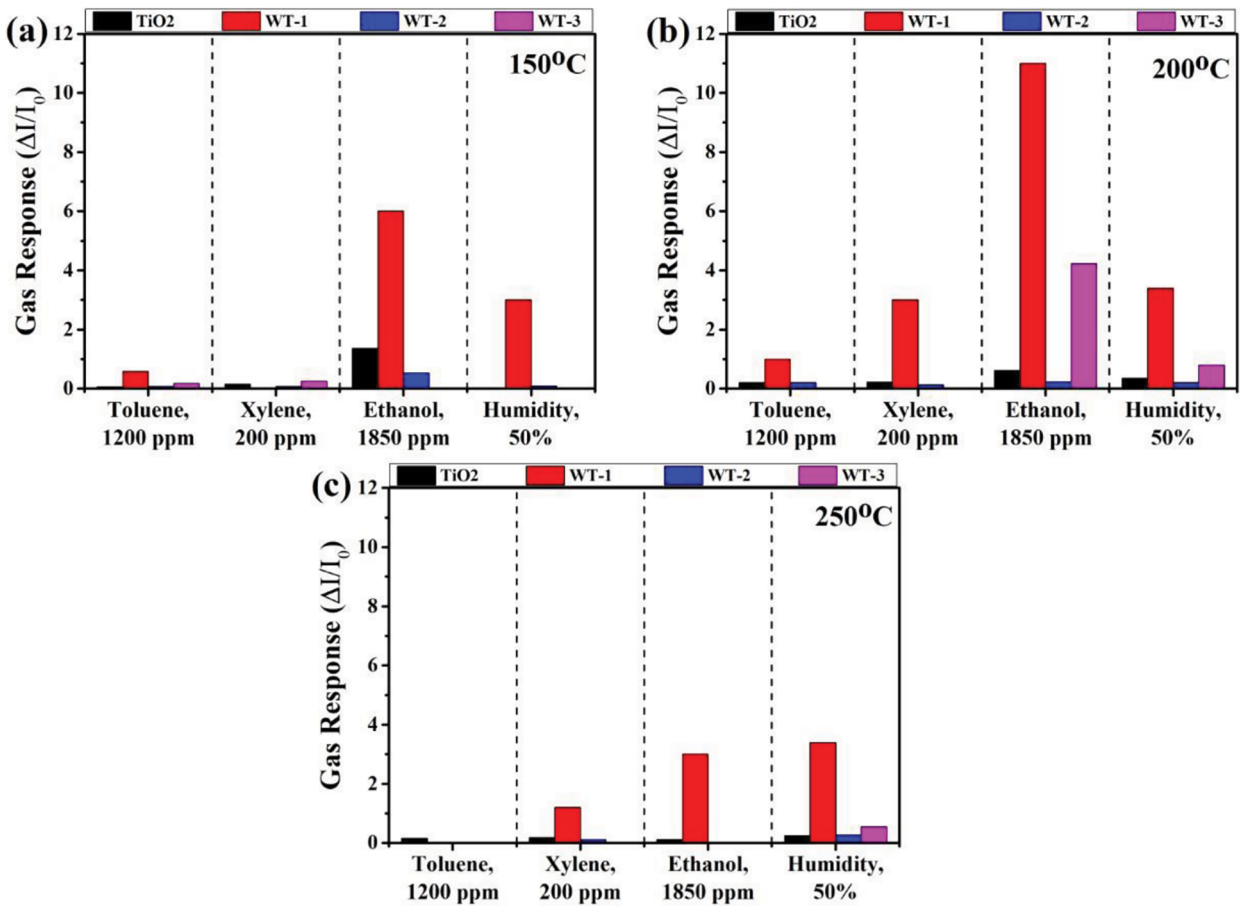

Figure 7. Sensor responses of samples at constant concentration against all tested gases at a) 150 °C, b) 200 °C, and c) 250 °C.

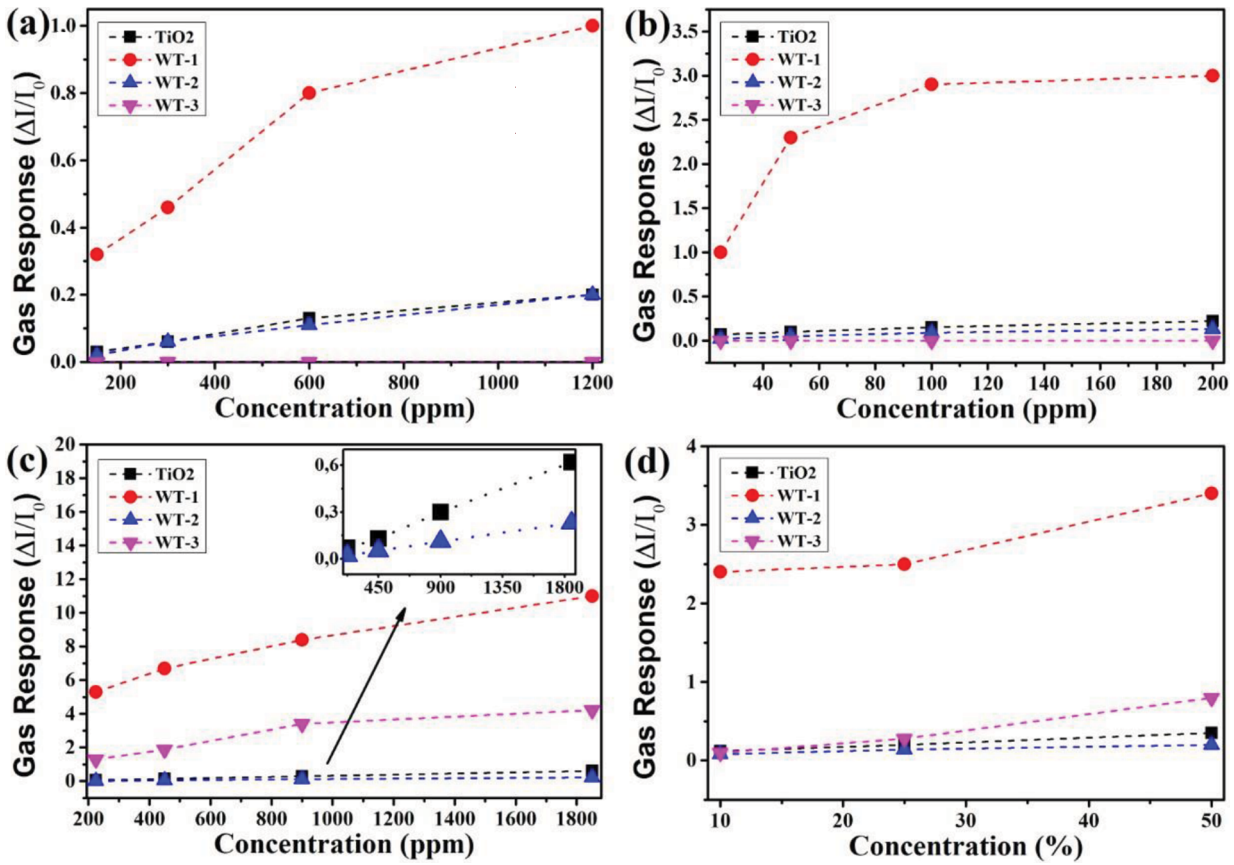

Figure 8. Gas concentration dependence of sensor response against a) toluene, b) xylene, c) ethanol, and d) relative humidity at 200 °C.

The sensing performances of aromatic compounds such as toluene and xylene change by increasing amount of loaded WO_3-layer on the TiO_2 NRs as seen in Figures 8a and 8b. Sensing performances of pristine TiO_2 NRs are similar toward 1200 ppm toluene (sensor response = 0.2) and 200 ppm xylene (sensor response = 0.22) and decrease linearly by decreasing concentration of the aromatic compounds. The best sensing responses of aromatic compounds were shown by WT-1 sensor. Moreover, WT-1 sensor has saturated by increasing of concentration as clearly seen in xylene sensing performance. At low concentrations, the sensor response increases rapidly against xylene and changes slowly by increasing concentration after 100 ppm. The sensor response against aromatic compounds of WT-2 less than WT-1. Moreover, WT-3 sensor could not sense toluene and xylene. Fabricated sensors show good linear characteristics in a certain concentration range of ethanol as seen in Figure 8c. Sensor response value increases with the increment of ethanol concentration. Figure 8d shows sensor response of samples against different relative humidity concentrations at 200 °C. WT-1 sample exhibited the highest sensor response at every concentration of relative humidity.

The investigation of concentration dependence of sensor response demonstrate that all sensors are most sensitive against ethanol molecules at optimal operation temperature. Sensor response of all samples against 1850 ppm ethanol and different ethanol concentrations for WT-1 sample at 200 °C are given in Figure 9.

It's clear that the signal returns to baseline after turning off the ethanol and purging with dry air. WO_3 modified TiO_2 NRs heterostructures showed enhanced sensor properties compared to the pristine TiO_2 NRs sensor. Sensing mechanisms of MOX sensors that are composed of only one type of materials have been studied and well explained in the literature [57,58]. Enhanced sensor properties can be attributed to the catalytic effect of WO_3. In this case, WO_3 plays a role as a catalyst material in the reaction between analyte gas and TiO_2. If the surface coverage of the WO_3 increase, the catalytic role of the WO_3 turns into a sensing layer, so a lower sensor performance generally is observed [59]. In Figure 3, SEM data also clarifies more coverage on the surface for WT-2 and WT-3. Previous works have also reported the enhanced sensor properties due to the catalyst role in heterostructures [17, 60-62]. WT-1 sample exhibited enhanced ethanol response than others and its concentration dependence sensor response performance was illustrated separately in Figure 9b. During the exposure, the response increased rapidly, then the rate of increment stopped and slightly declined to reach the saturation.

While purging the sensor, the response decreases rapidly and reaches baseline. Response times ($t90_{res}$) of WT-1 sensor are 6 min for each ethanol concentrations. The sensor showed a very stable sensing characteristic against ethanol. On the other hand, recovery times ($t90_{rec}$) of WT-1 sensor are 15, 14, 8, and 6 min for 1850, 900, 450, and 225 ppm ethanol, respectively. These time values are better than the ones in our previous ethanol sensor studies [22,50].

SMO materials such as TiO_2 and WO_3 have oxygen deficiencies on crystalline surface due to their specific stoichiometry. As a result of this condition, free electrons appear in the conduction band of SMO material. Therefore, this type of semiconductors is named as n-type semiconductor. Gas sensing mechanism of n-type SMO materials generally can be explained with oxygen adsorption on the surface as given in Figure 10. When the n-type SMO was exposed to ambient, oxygen molecules in the air would be adsorbed on the surface of SMO with capturing by charge carriers (free electrons) (Figure 10a). Decrease in number of charge carriers leads to appearance of depletion layer between the grain boundaries that limits the electron transfer. Therefore, the depletion layer width and contact barrier height between two adjacent grains will be increased by the remaining number of oxygen molecules. The higher contact barrier leads to lower conductance of n-type SMO. When n-type SMO material is exposed to reducing gas molecules, these molecules react with the preadsorbed oxygen molecules (Figure 10b). Then, the depletion layer width and contact barrier height between two adjacent grains decreases again. As a result, this reaction leads to increasing of n-type SMO materials conductance [63].

When there is contact formed between TiO_2 and WO_3, these two different n-type SMO materials behave as a new sensing material named as n-WO_3/n-TiO_2 heterostructure, as shown in Figure 11. Because Fermi levels of TiO_2 is higher

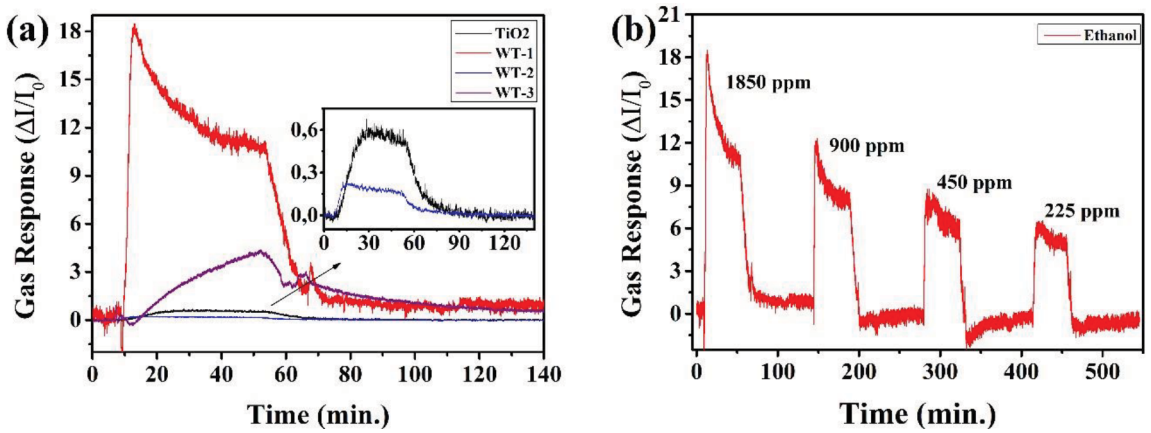

Figure 9. a) Sensor response of 1850 ppm ethanol for all samples and b) different ethanol concentrations for WT-1 sample at 200 °C.

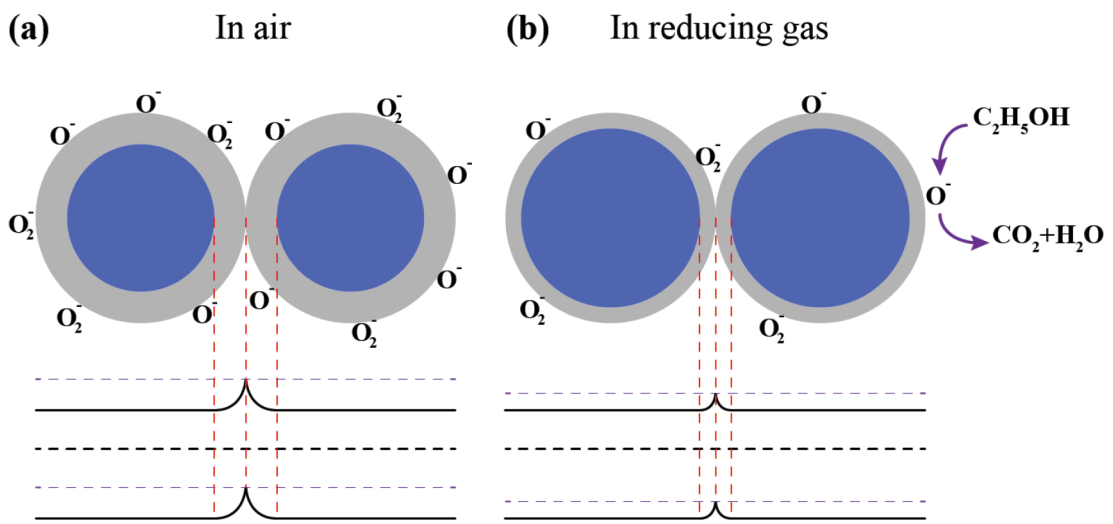

Figure 10. The schematic illustration of n-type metal oxide gas sensors grain boundary when exposed to a) air ambient and b) reducing gas ambient.

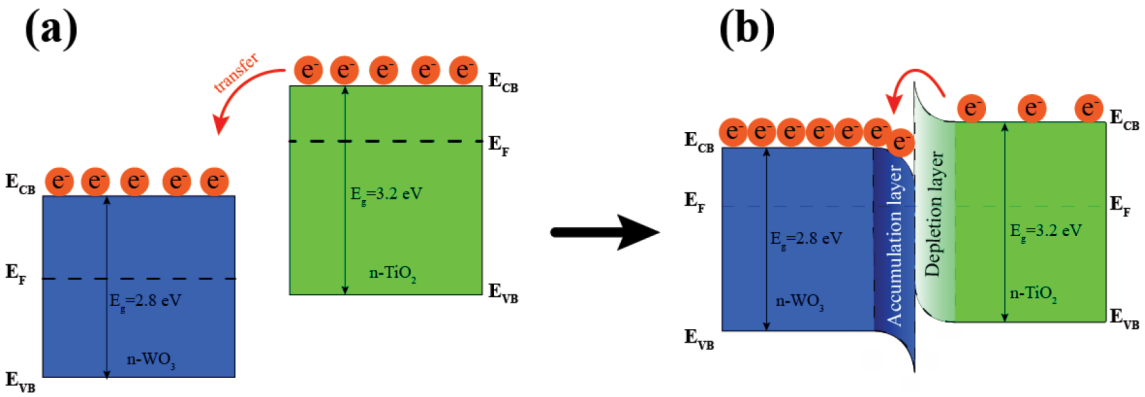

Figure 11. Energy band diagram of a) n-type TiO_2 and n-type WO_3 with different Fermi levels and direction of electrons migration to reach thermal equilibrium; b) formation of n-WO_3/n-TiO_2 heterostructure with accumulation and depletion layer.

than that of WO_3, the electrons are transferred from conduction band of TiO_2 to the conduction band of WO_3 (Figure 11a). This process would continue until equalising of the Fermi level between WO_3 and TiO_2 occurs. The formation of n-n-type heterostructure leads to the creation of an electron depletion layer in TiO_2 and an electron accumulation layer in WO_3 (Figure 11b). The accumulation layer of WO_3 would be enhanced oxygen adsorption in air ambient [40,48-50,64].

4. Conclusion

WO_3/TiO_2 heterostructures were fabricated to investigate VOCs sensing performance. According to morphological characterisation, WO_3 uniformly covered the entire highly ordered TiO_2 NRs surface. XRD investigation shows that TiO_2 NRs was grown on rutile phase and was highly aligned along the [001] direction. XRD peaks of WO_3 on samples did not exist due to their small amounts. However, further investigation illustrated that WO_3 will grow in monoclinic phase with the thermal oxidation method. TiO_2 and WO_3/TiO_2 heterostructures were tested against VOCs such as toluene, xylene, acetone and ethanol, and relative humidity. It was observed that n-n-type WO_3/TiO_2 heterostructure advanced the sensor performance of TiO_2 NRs against almost all tested gases, except acetone, which is not detected with any sensors. WT-1 sensor showed the best sensor performance compared to TiO_2, WT-2 and WT-3 sensors. Ethanol sensing response of WT-1 sensor was 18-fold higher than pristine TiO_2 NRs at 200 °C. The enhanced gas sensor performance of WO_3/TiO_2 heterostructure is attributed to n-n type heterostructure formation that leads to the formation of depletion and accumulation layers. According to our findings, n-WO_3/n-TiO_2 heterostructures have a high potential for ethanol sensor applications.

References

1. Cui P, Schito G, Cui Q. VOC emissions from asphalt pavement and health risks to construction workers. Journal of Cleaner Production 2020; 244: 118757.
2. Liu Y, Shao M, Fu L, Lu S, Zeng L et al. Source profiles of volatile organic compounds (VOCs) measured in China: part I. Atmospheric Environment. 2008; 42 (25): 6247-6260.
3. Manisalidis I, Stavropoulou E, Stavropoulos A, Bezirtzoglou E. Environmental and health impacts of air pollution: a review. Frontiers in Public Health 2020; 8.
4. Nabizadeh R, Sorooshian A, Delikhoon M, Baghani AN, Golbaz S et al. Characteristics and health effects of volatile organic compound emissions during paper and cardboard recycling. Sustainable Cities and Society 2020; 56: 102005.
5. Pekey B, Yılmaz H. The use of passive sampling to monitor spatial trends of volatile organic compounds (VOCs) at an industrial city of Turkey. Microchemical Journal 2011; 97 (2): 213-219.
6. Xie Y, Berkowitz CM. The use of positive matrix factorization with conditional probability functions in air quality studies: an application to hydrocarbon emissions in Houston, Texas. Atmospheric Environment 2006; 40 (17): 3070-3091.
7. Buszewski B, Kęsy M, Ligor T, Amann A. Human exhaled air analytics: biomarkers of diseases. Biomedical Chromatography. 2007; 21 (6): 553-566.

8. Kim K-H, Jahan SA, Kabir E. A review of breath analysis for diagnosis of human health. Trends in Analytical Chemistry 2012; 33: 1-8.

9. Popov TA. Human exhaled breath analysis. Annals of Allergy, Asthma & Immunology 2011; 106 (6): 451-456.

10. Jones A. Excretion of low-molecular weight volatile substances in human breath: focus on endogenous ethanol. Journal of Analytical Toxicology 1985; 9 (6): 246-250

11. Blohm A, Sieburg A, Popp J, Frosch T. Detection of gas molecules by means of spectrometric and spectroscopic methods. Advanced Nanostructures for Environmental Health: Elsevier; 2020. p. 251-294

12. Cernosek T, Eckert KE, Carter DO, Perrault KA. Volatile organic compound profiling from postmortem microbes using gas chromatography–mass spectrometry. Journal of Forensic Sciences 2020; 65 (1): 134-143

13. Elosúa C, Bariáin C, Matías IR, Arregui FJ, Luquin A et al. Volatile alcoholic compounds fibre optic nanosensor. Sensors and Actuators B: Chemical 2006; 115 (1): 444-449.

14. Guha P, Santra S, Gardner J. Integrated CMOS-based sensors for gas and odor detection. Semiconductor Gas Sensors: Elsevier; 2020. p. 465-487.

15. Mirzaei A, Leonardi S, Neri G. Detection of hazardous volatile organic compounds (VOCs) by metal oxide nanostructures-based gas sensors: a review. Ceramics international 2016; 42 (14): 15119-15141.

16. Sureshkumar N, Dutta A. Environmental gas sensors based on nanostructured thin films. Multilayer thin films-versatile applications for materials engineering: IntechOpen; 2020.

17. Alev O, Kılıç A, Çakırlar Ç, Büyükköse S, Öztürk ZZ. Gas sensing properties of p-Co_3O_4/n-TiO_2nanotube heterostructures. Sensors 2018; 18 (4): 956.

18. Alev O, Sarıca N, Özdemir O, Arslan LÇ, Büyükköse S et al. Cu-doped ZnO nanorods based QCM sensor for hazardous gases. Journal of Alloys and Compounds 2020; 826: 154177.

19. Fu Z, Zhang G, Tang Z, Zhang H. Preparation and application of ordered mesoporous metal oxide catalytic materials. Catalysis Surveys from Asia 2020; 24 (1): 38-58.

20. Lee J-H, Mirzaei A, Kim J-Y, Kim J-H, Kim HW et al. Optimization of the surface coverage of metal nanoparticles on nanowires gas sensors to achieve the optimal sensing performance. Sensors and Actuators B: Chemical 2020; 302: 127196.

21. Sarıca N, Alev O, Arslan LÇ, Öztürk ZZ. Characterization and gas sensing performances of noble metals decorated CuO nanorods. Thin Solid Films 2019; 685: 321-328.

22. Şennik E, Alev O, Öztürk ZZ. The effect of Pd on the H_2 and VOC sensing properties of TiO_2 nanorods. Sensors and Actuators B: Chemical 2016; 229: 692-700.

23. Alev O, Şennik E, Kılınç N, Öztürk ZZ. Gas sensor application of hydrothermally growth TiO_2 nanorods. Procedia Engineering 2015; 120: 1162-1165.

24. Maziarz W, Kusior A, Trenczek-Zajac A. Nanostructured TiO_2-based gas sensors with enhanced sensitivity to reducing gases. Beilstein Journal of Nanotechnology 2016; 7 (1): 1718-1726.

25. Sennik E, Kilinc N, Ozturk ZZ. Electrical and VOC sensing properties of anatase and rutile TiO_2 nanotubes. Journal of Alloys and Compounds 2014; 616: 89-96.

26. Seo M-H, Yuasa M, Kida T, Kanmura Y, Huh J-S et al. Gas sensor using noble metal-loaded TiO_2 nanotubes for detection of large-sized volatile organic compounds. Journal of the Ceramic Society of Japan 2011; 119 (1395): 884-889.

27. Teleki A, Pratsinis SE, Kalyanasundaram K, Gouma P. Sensing of organic vapors by flame-made TiO_2 nanoparticles. Sensors and Actuators B: Chemical 2006; 119 (2): 683-90.

28. Alev O, Şennik E, Öztürk ZZ. Improved gas sensing performance of p-copper oxide thin film/n-TiO_2 nanotubes heterostructure. Journal of Alloys and Compounds 2018; 749: 221-228.

29. Avansi Jr W, Catto AC, Da Silva LF, Fiorido T, Bernardini S et al. One-dimensional V_2O_5/TiO_2 heterostructures for chemiresistive ozone sensors. ACS Applied Nano Materials 2019; 2 (8): 4756-1764.

30. Deng J, Wang L, Lou Z, Zhang T. Design of CuO-TiO_2 heterostructure nanofibers and their sensing performance. Journal of Materials Chemistry A 2014; 2 (24): 9030-9034.

31. Lyson-Sypien B, Kusior A, Rekas M, Zukrowski J, Gajewska M et al. Nanocrystalline TiO_2/SnO_2 heterostructures for gas sensing. Beilstein Journal of Nanotechnology 2017; 8 (1): 108-122.

32. Wang Y, Wu T, Zhou Y, Meng C, Zhu W et al. TiO_2-based nanoheterostructures for promoting gas sensitivity performance: designs, developments, and prospects. Sensors 2017; 17 (9): 1971.

33. Kanda K, Maekawa T. Development of a WO_3 thick-film-based sensor for the detection of VOC. Sensors and Actuators B: Chemical 2005; 108 (1-2): 97-101.

34. Vallejos S, Khatko V, Calderer J, Gracia I, Cané C et al. Micro-machined WO_3-based sensors selective to oxidizing gases. Sensors and Actuators B: Chemical 2008; 132 (1): 209-215.

35. Liu Y, Xie C, Li H, Chen H, Zou T, Zeng D. Improvement of gaseous pollutant photocatalysis with WO_3/TiO_2 heterojunctional-electrical layered system. Journal of Hazardous Materials 2011; 196: 52-58.

36. Prabhu S, Nithya A, Mohan SC, Jothivenkatachalam K (editors). Synthesis, surface acidity and photocatalytic activity of WO_3/TiO_2 nanocomposites – an overview. Materials Science Forum; 2014; 781: 63-78.

37. Tang K, Zhang Y, Shi Y, Cui J, Shu X et al. Fabrication of WO_3/TiO_2 core-shell nanowire arrays: structure design and high electrochromic performance. Electrochimica Acta 2020; 330: 135189.

38. Depero L, Ferroni M, Guidi V, Marca G, Martinelli G et al. Preparation and micro-structural characterization of nanosized thin film of TiO_2-WO_3 as a novel material with high sensitivity towards NO_2. Sensors and Actuators B: Chemical 1996; 36 (1-3): 381-383.

39. Lee DS, Han SD, Lee SM, Huh JS, Lee DD. The TiO_2-adding effects in WO_3-based NO_2 sensors prepared by coprecipitation and precipitation method. Sensors and Actuators B: Chemical 2000; 65 (1-3): 331-335.

40. Yao Y, Yuan J, Chen X, Tan L, Gu Q et al. In situ construction and sensing mechanism of TiO_2–WO_3 composite coatings based on the semiconductor heterojunctions. Journal of Materials Research and Technology 2019; 8 (4): 3580-8358.

41. Zanetti S, Rocha K, Rodrigues J, Longo E. Soft-chemical synthesis, characterization and humidity sensing behavior of WO_3/TiO_2 nanopowders. Sensors and actuators B: Chemical 2014; 190: 40-47.

42. Meng W, Dai L, Zhu J, Li Y, Meng W et al. A novel mixed potential NH_3 sensor based on TiO_2@ WO_3 core-shell composite sensing electrode. Electrochimica Acta 2016; 193: 302-310.

43. Zappa D, Galstyan V, Kaur N. Munasinghe Arachchige HMM, Sisman O, Comini E. Metal oxide -based heterostructures for gas sensors- a review. Analytica Chimica Acta 2018; 1039: 1-23.

44. Walker JM, Akbar SA, Morris PA. Synergistic effects in gas sensing semiconducting oxide nano-heterostructures: A review. Sensors and Actuators B: Chemical 2019; 286: 624-640.

45. Moseley PT. Progress in the development of semiconducting metal oxide gas sensors: a review. Measurement Science and Technology 2017; 28 (8): 082001.

46. Feng X, Shankar K, Varghese OK, Paulose M, Latempa TJ et al. Vertically aligned single crystal TiO_2 nanowire arrays grown directly on transparent conducting oxide coated glass: Synthesis details and applications. Nano Letters 2008; 8 (11).

47. Astinchap B, Moradian R, Gholami K. Effect of sputtering power on optical properties of prepared TiO_2 thin films by thermal oxidation of sputtered Ti layers. Materials Science in Semiconductor Processing 2017; 63: 169-175.

48. Xiao G, Shi C, Li L, Zhang Z, Ma C et al. A 200-nm length TiO_2 nanorod array with a diameter of 13 nm and areal density of 1100 μm^{-2} for efficient perovskite solar cells. Ceramics International 2017; 43 (15): 12534-12539.

49. Altomare M, Nguyen NT, Hejazi S, Schmuki P. A Cocatalytic electron- transfer cascade site- selectively placed on TiO_2 nanotubes yields enhanced photocatalytic H_2evolution. Advanced Functional Materials 2018; 28 (2): 1704259.

50. Şennik E, Soysal U, Öztürk ZZ. Pd loaded spider-web TiO_2 nanowires: fabrication, characterization and gas sensing properties. Sensors and Actuators B: Chemical 2014; 199: 424-432.

51. Lin CW, Huang KL, Chang KW, Chen JH, Chen KL et al. Ultraviolet photodetector and gas sensor based on amorphous In-Ga-Zn-O film. Thin Solid Films 2016; 618: 73-76.

52. Wu CH, Jiang GJ, Chang KW, Lin CW, Chen KL. Highly sensitive amorphous In–Ga–Zn–O films for ppb-level ozone sensing: effects of deposition temperature. Sensors and Actuators B: Chemical 2015; 211: 354-358.

53. Lai CW, Sreekantan S. Preparation of hybrid WO_3-TiO_2 nanotube photoelectrodes using anodization and wet impregnation: improved water-splitting hydrogen generation performance. International Journal of Hydrogen Energy 2013; 38 (5): 2156-2166.

54. Banerjee AN. The design, fabrication, and photocatalytic utility of nanostructured semiconductors: focus on TiO_2-based nanostructures. Nanotechnology, Science and Applications 2011; 4: 35.

55. Suryawanshi H, Patil D. Synthesis of nanostructure TiO_2 nanorod array on FTO substrate using hydrothermal method and its photocatalytic activity. International Journal for Research in Applied Science & Engineering Technology 2018; 6 (4): 48-53.

56. Meng X, Shin DW, Yu SM, Park MH, Yang C et al. Formation mechanism of rutile TiO_2 rods on fluorine doped tin oxide glass. Journal of Nanoscience and Nanotechnology 2014; 14 (11): 8839-8844.

57. Liu Y, Li G, Mi R, Deng C, Gao P. An environment-benign method for the synthesis of p-NiO/n-ZnO heterostructure with excellent performance for gas sensing and photocatalysis. Sensors and Actuators B: Chemical 2014; 191: 537-544.

58. Miller DR, Akbar SA, Morris PA. Nanoscale metal oxide-based heterojunctions for gas sensing: a review. Sensors and Actuators B: Chemical 2014; 204: 250-272.

59. Liu L, Guo C, Li S, Wang L, Dong Q et al. Improved H_2 sensing properties of Co-doped SnO_2 nanofibers. Sensors and Actuators B: Chemical 2010; 150 (2): 806-810.

60. Wöllenstein J, Burgmair M, Plescher G, Sulima T, Hildenbrand J et al. Cobalt oxide based gas sensors on silicon substrate for operation at low temperatures. Sensors and Actuators B: Chemical 2003; 93 (1): 442-448.

61. Liu PF, Yang S, Zheng LR, Zhang B, Yang HG. Electrochemical etching of α-cobalt hydroxide for improvement of oxygen evolution reaction. Journal of Materials Chemistry A 2016; 4 (24): 9578-9584.

62. Kohl D. Function and applications of gas sensors. Journal of Physics D: Applied Physics 2001; 34 (19): R125-R49.

63. Xu C, Tamaki J, Miura N, Yamazoe N. Grain size effects on gas sensitivity of porous SnO_2-based elements. Sensors and Actuators B: Chemical 1991; 3 (2): 147-155.

64. Ali H, Ismail N, Hegazy A, Mekewi M. A novel photoelectrode from TiO_2-WO_3 nanoarrays grown on FTO for solar water splitting. Electrochimica Acta 2014; 150: 314-319.